ELSEVIER

Journal of the Mechanics and Physics of Solids
51 (2003) 2169–2190

JOURNAL OF THE
MECHANICS AND
PHYSICS OF SOLIDS

www.elsevier.com/locate/jmps

Kinetics of crack initiation and growth in organic-containing integrated structures☆

Z. Suo[a,*], J.H. Prévost[b], J. Liang[c]

[a] *Division of Engineering and Applied Sciences, Harvard University, Cambridge, MA 02138, USA*
[b] *Civil and Environmental Engineering Department, Princeton University, Princeton, NJ 08544, USA*
[c] *Intel Corporation, 2501 NW 229th Avenue, Mailstop RA3-355, Hillsboro, OR 97124, USA*

Abstract

Organic materials are being introduced into solid-state devices to enhance performance, reduce cost, or add function. In such an integrated structure, creep in the organic material affects cracking in the adjacent inorganic material. This paper analyzes an idealized structure comprising, from top to bottom, an inorganic film, an organic underlayer, and a rigid substrate. The film is elastic, subject to a tensile stress, and susceptible to subcritical crack growth. The underlayer is viscoelastic and does not crack. A crack exists in the film. When the crack tip is stationary, as the underlayer creeps, the film stress relaxes in the crack wake, but intensifies around the crack tip, so that the crack may grow after a delay. When the crack tip moves, the underlayer creeps to a limited extent, and constrains the fresh crack opening. A nonequilibrium thermodynamic model evolves displacements, creep strains, and crack length simultaneously. Using the Laplace transform and the extended finite element method, we study delayed crack initiation, steady crack growth, and transient crack growth.

Keywords: Thin film; Fracture; Subcritical cracking; Viscoelasticity; Polymers

1. Introduction

Solid-state devices are structures with complex architectures, diverse materials, and small feature sizes. Their fabrication, function, and reliability pose serious questions,

☆ This paper is prepared for a symposium held at Caltech, 16–18 January 2003 and a special issue of *Journal of the Mechanics and Physics of Solids* organized by A.J. Rosakis, G. Ravichandran, and S. Suresh to celebrate the 60th birthday of Professor L.B. Freund.

* Corresponding author. Tel.: +1-617-495-3789; fax: +1-617-496-0601.
E-mail address: suo@deas.harvard.edu (Z. Suo).

0022-5096/$ - see front matter © 2003 Elsevier Ltd. All rights reserved.
doi:10.1016/j.jmps.2003.09.022

motivating an active field of study in mechanics and materials (Freund, 2000). Representative topics include plasticity in small structures (Nix, 1989; Arzt, 1998), fracture in layered materials (Hutchinson and Suo, 1991; Hutchinson and Evans, 2000), thin film adhesion (Evans and Hutchinson, 1995; Dauskardt et al., 1998; Volinsky et al., 2002), dislocations in epitaxial growth (Freund, 1994), evolving small structures (Suo, 1997), self-assembled quantum dots (Gao and Nix, 1999), and interconnect reliability (Suo, 2003). A textbook of thin film mechanics is due out this year (Freund and Suresh, 2003).

Recently, intense activities have emerged worldwide to integrate organic materials into solid-state devices. Some of the state-of-the-art interconnect structures, for example, use a low-dielectric-constant polymer to allow microprocessors to operate at high speeds (Martin et al., 2000). Light-emitting devices are now also made with polymers and small-molecule organics (Forrest, 1997). Transistors are fabricated directly on polymer substrates to make deformable devices (Gleskova et al., 1999; Cairns et al., 2000; Hsu et al., 2002).

In addition to the organic materials, the devices contain other materials, some of which are brittle, including silicon nitride as an etch stop or a passivation, amorphous and polycrystalline silicon in thin-film transistors, tin-doped indium oxide as a transparent conductor, and ubiquitous silicon dioxide. After operation for some time, the devices may fail when the brittle materials crack. Why does creep in organic materials affect device lifetime? How can accelerated reliability tests be interpreted?

This paper studies an idealized structure, comprising an inorganic film, an organic underlayer, and a rigid substrate (Fig. 1). The film is elastic, subject to a tensile stress, and susceptible to subcritical crack growth. The underlayer is viscoelastic and does not crack. The film and the underlayer remain bonded. A flaw in the film may grow into a channel crack. Time-independent channel cracks have been studied by, e.g., Hu and Evans (1989), Hutchinson and Suo (1991), Beuth (1992), Beuth and Klingbeil (1996), and Ambrico et al. (2002). Compared to a crack in a free-standing sheet, the channel crack has its opening constrained by the underlayer. In the present structure, the constraint is gradually lost as the underlayer creeps.

The tri-layer structure in Fig. 1 leads to an attractive model, which has appeared in diverse applications. In a study of tectonic plate motion, Rice (1980) and Lehner et al. (1981) modeled the lithosphere as an elastic layer, and the asthenosphere as a Maxwell viscoelastic underlayer. The model, with a viscous underlayer, was used to study stress diffusion in the lithosphere (Elsasser, 1969), in electronic packages (He et al., 1998), and in semiconductor islands (Freund and Nix, unpublished; Huang et al., 2001; Moran and Kuech, 2001; Sridhar et al., 2002). Xia and Hutchinson (2000), and Liang et al. (2003a) used the model to study crack patterns in a brittle film on an elastic underlayer. A similar study was carried out for a viscous underlayer (Huang et al., 2002a; Liang et al., 2003b). Assuming that the underlayer is elastic and plastic, Huang et al. (2002b) developed a theory of ratcheting-induced stable cracking (RISC).

Building on the previous work, this paper studies the kinetics of crack initiation and growth. Section 2 outlines the model. Section 3 discusses the glassy and the rubbery limits of the underlayer, leading to a classification of crack behaviors.

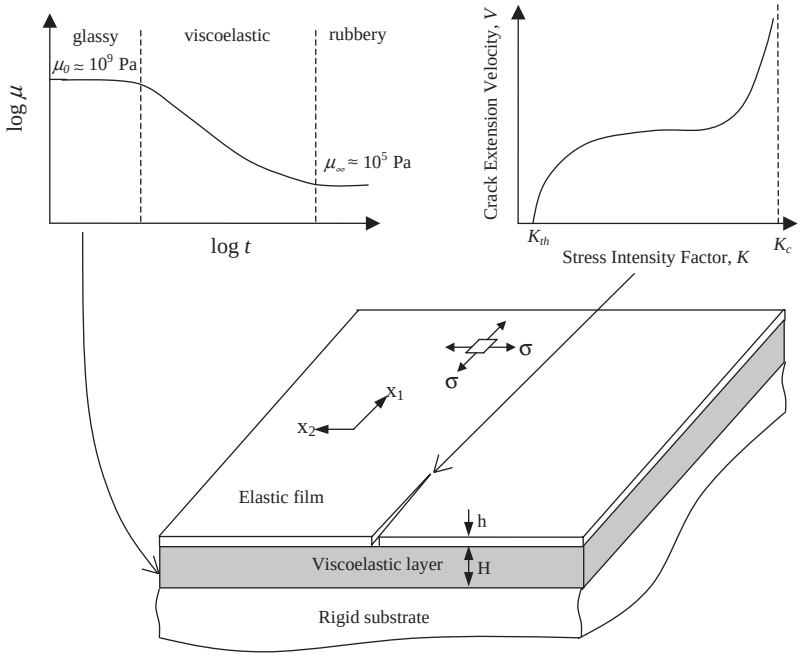

Fig. 1. A schematic of a tri-layer structure. The underlayer is viscoelastic, with the shear modulus decreases as a function of time. The film is susceptible to subcritical crack growth, with the crack velocity increases with the stress intensity factor.

Section 4 studies crack initiation. When the crack tip is stationary, as the underlayer creeps, the stress builds up around the crack tip. The stress intensity factor as a function of time, calculated using the Laplace transform, determines the delay time for the crack to initiate growth. Sections 5 and 6 study steady and transient crack growth. When the crack tip moves, the underlayer has little time to creep, and constrains the fresh crack opening. The appendix re-formulates the model within a framework of nonequilibrium thermodynamics, leading to a finite element method.

2. The model of co-evolution

The crack and the underlayer co-evolve. The crack extends to allow the underlayer to creep over a large extent. The underlayer, in turn, creeps to allow the stress to build up at the crack tip. The elastic energy stored in the film drives the evolution. The two rate processes, crack growth and underlayer creep, dissipate energy. These statements are made precise in the appendix, within the framework of nonequilibrium thermodynamics. This section outlines the model in more familiar terms.

2.1. Viscoelastic deformation

As illustrated in Fig. 1, the film is an infinite sheet, with its surface coinciding with the coordinate plane (x_1, x_2). At time $t < 0$, the film is under a uniform biaxial tensile stress of magnitude σ. A perfect film would remain in this state forever. If a crack is introduced in the film at $t = 0$, however, the stress field evolves with time t. As the underlayer creeps, the film stress relaxes in the crack wake, and builds up around the crack tip. For a crack long compared to the film and underlayer thickness, and an underlayer compliant compared to the film, we assume that the film deforms in the plane stress conditions, and the underlayer deforms in pure shear. Denote the membrane stresses in the film by $\sigma_{\alpha\beta}(x_1, x_2, t)$, and the shear stresses in the underlayer by $\tau_\alpha(x_1, x_2, t)$. The Greek subscripts take on the values 1 and 2.

The film and the underlayer are well bonded, so that the shear stresses in the underlayer act on the bottom surface of the film. Let h be the film thickness. The deformation is taken to be so slow that the inertia effect is negligible. Force balance of a differential element of the film, $(\mathrm{d}x_1, \mathrm{d}x_2, h)$, requires that

$$\sigma_{\alpha\beta,\beta} = \tau_\alpha / h. \tag{1}$$

The repeated Greek subscript implies summation over 1 and 2, and the comma between the subscripts denotes partial differentiation. The quantity, $-\tau_\alpha/h$, acts like a body force in the plane of the film.

The displacements in the plane of the film are set to zero when the film is in the state of uniform stress, $\sigma_{\alpha\beta} = \sigma\delta_{\alpha\beta}$, and are denoted by $u_\alpha(x_1, x_2, t)$ at time t. The in-plane strains are

$$\varepsilon_{\alpha\beta} = \frac{1}{2}(u_{\alpha,\beta} + u_{\beta,\alpha}). \tag{2}$$

The film is linear elastic. Under the plane stress conditions, Hooke's law relates the stresses and strains as

$$\sigma_{\alpha\beta} = \sigma\delta_{\alpha\beta} + \bar{E}[(1-v)\varepsilon_{\alpha\beta} + v\varepsilon_{\gamma\gamma}\delta_{\alpha\beta}], \tag{3}$$

where E is Young's modulus of the film, v is Poisson's ratio of the film, and $\bar{E} = E/(1-v^2)$. The first term on the right hand side of Eq. (3) is the biaxial residual stress.

The underlayer, thickness H, is bonded to the film at one interface, and to the rigid substrate at the other. The shear strains $\gamma_\alpha(x_1, x_2, t)$ in the underlayer relate to the in-plane displacements of the film:

$$\gamma_\alpha = u_\alpha / H. \tag{4}$$

The underlayer is viscoelastic, representative of a cross-linked polymer. When the material is subject to a sudden shear strain γ at time $t = 0^+$, holding the strain constant in the subsequent time, the shear stress rises suddenly, and then relaxes according to $\tau = \mu(t)\gamma$. The relaxation function, $\mu(t)$, is sketched in Fig. 1, with the glassy modulus $\mu(0) = \mu_0$, and the rubbery modulus $\mu(\infty) = \mu_\infty$. Boltzmann's superposition principle relates the shear stresses to an arbitrary history of the shear strains (Christensen, 1982):

$$\tau_\alpha(x_1, x_2, t) = \int_{-\infty}^{t} \mu(t - t') \frac{\partial \gamma_\alpha(x_1, x_2, t')}{\partial t'} \, \mathrm{d}t'. \tag{5}$$

Eq. (5) recovers two special cases. When the underlayer is elastic, the shear stresses relate to the shear strains as $\tau_\alpha = \mu\gamma_\alpha$, where the shear modulus μ is independent of time. When the underlayer is viscous, the shear stresses relate to the shear strain-rates as $\tau_\alpha = \eta\partial\gamma_\alpha/\partial t$, where η is the viscosity of the underlayer, and the relaxation modulus is a delta function, $\mu(t) = \eta\delta(t)$.

A combination of Eqs. (1)–(5) gives the field equation for the displacements:

$$\bar{E}\left[\frac{1-v}{2}u_{\alpha,\beta\beta} + \frac{1+v}{2}u_{\beta,\beta\alpha}\right] = \frac{1}{hH}\int_{-\infty}^{t}\mu(t-t')\frac{\partial u_\alpha(x_1,x_2,t')}{\partial t'}\,\mathrm{d}t'. \tag{6}$$

The traction-free conditions hold at the crack faces, $\sigma_{\alpha\beta}n_\beta = 0$, where n_β are the components of the unit vector normal to the crack faces. In terms of the displacement gradient, the boundary conditions become

$$\sigma n_\alpha + \bar{E}\left[\frac{1-v}{2}(u_{\alpha,\beta} + u_{\beta,\alpha}) + vu_{\gamma,\gamma}\delta_{\alpha\beta}\right]n_\beta = 0. \tag{7}$$

2.2. Subcritical crack growth

At time t, the coordinates of the crack tip are $x_1 = a_1(t)$ and $x_2 = a_2(t)$. Let $(\bar{x}_1,\bar{x}_2)$ be the moving frame whose origin coincides with the crack tip. A material particle (x_1,x_2) has the coordinates $\bar{x}_\alpha = x_\alpha - a_\alpha(t)$ in the moving frame. Eq. (5) becomes

$$\tau_\alpha(\bar{x}_1,\bar{x}_2,t) = \frac{1}{H}\int_{-\infty}^{t}\mu(t-t')\left[\frac{\partial u_\alpha(\bar{x}_1,\bar{x}_2,t')}{\partial t'} - \frac{\partial u_\alpha(\bar{x}_1,\bar{x}_2,t')}{\partial \bar{x}_\beta}\frac{\mathrm{d}a_\beta(t')}{\mathrm{d}t'}\right]\mathrm{d}\xi. \tag{8}$$

At the crack tip, the stress field is singular in $\bar{x}_1$ and $\bar{x}_2$, but smooth in t; the displacement field is bounded. The terms $\partial u_\alpha(\bar{x}_1,\bar{x}_2,t')/\partial t'$ are bounded, but the terms $\partial u_\alpha(\bar{x}_1,\bar{x}_2,t')/\partial \bar{x}_\beta$ are singular, so that the shear stresses τ_α are singular. However, the terms $\partial u_\alpha(\bar{x}_1,\bar{x}_2,t')/\partial \bar{x}_\beta$ are one order less singular than the terms on left-hand side of Eq. (6). Consequently, the structure of the singular crack tip field is unaffected by the shear stresses in the underlayer, and is the same as that of a crack in an elastic body, under the plane stress conditions, with no body force.

We will consider a mode I crack growing along the x_1-axis. Let (r,θ) be the polar coordinates centered at the crack tip. The leading terms of the stress and the displacement fields around the crack tip take the well-known forms

$$\sigma_{\alpha\beta}(r,\theta,t) = \frac{K(t)}{\sqrt{2\pi r}}\Sigma_{\alpha\beta}(\theta), \tag{9}$$

$$u_\alpha(r,\theta,t) = \frac{K(t)}{E}\sqrt{\frac{r}{2\pi}}\,U_\alpha(\theta). \tag{10}$$

The functions $\Sigma_{\alpha\beta}(\theta)$ and $U_\alpha(\theta)$ are given in Lawn (1993). The singular field depends on time only through the stress intensity factor, $K(t)$.

A crack in a brittle solid is susceptible to subcritical growth, assisted by thermal energy and molecules in the environment. The atomic bonds do not break when the stress intensity factor is below a threshold value K_{th}, and break instantaneously when

the stress intensity factor approaches a critical value K_c. When the stress intensity factor K falls in the intermediate regime, $K_{th} < K < K_c$, the atomic bonds break at a finite rate, and the crack velocity is a function of the stress intensity factor:

$$\frac{da}{dt} = V(K). \tag{11}$$

The trend of this function is sketched in Fig. 1. The subcritical crack growth law has been measured for bulk materials (Lawn, 1993), and for thin films (Ma et al., 1998; Cook and Liniger, 1999; He, 2002; McElhaney and Ma, 2003).

It is instructive to compare the present problem with two well-studied problems. For a crack moving at a high velocity so that the inertia effect is important, the acceleration of material particles (i.e., the second order time derivative of the displacement) enters, and the singular stress field depends on the crack velocity (Freund, 1990). For a crack with its tip in a viscoelastic solid, even when the stress intensity factor is constant, the displacement field changes with time, so that the stress intensity factor by itself does not characterize the crack tip field (Knauss, 1970). By contrast, in the present problem, the inertia effect is negligible and the crack tip is in an elastic solid, so that the stress intensity factor alone characterizes the crack tip field. The subcritical crack growth law, $V(K)$, is specific to the brittle film and the environmental molecules, but is independent of the underlayer. Creep in the underlayer modulates the crack behavior by affecting the stress intensity factor K.

3. Glassy and rubbery limits: classification of crack behaviors

The two functions, $\mu(t)$ and $V(K)$, which characterize the rate processes, vary with materials, temperature, and molecular species and concentrations in the environment. Nonetheless a classification of crack behaviors can be made on the basis of a small set of parameters: the glassy modulus μ_0, the rubbery modulus μ_∞, the threshold stress intensity factor K_{th}, and the critical stress intensity factor K_c.

3.1. Elastic underlayer

This sub-section reviews the Xia-Hutchinson (2000) solution for a crack in a film on an elastic underlayer, a special case that plays several roles in this paper. When the underlayer is elastic, with $\tau_\alpha = \mu\gamma_\alpha$, a combination of Eqs. (1)–(4) gives the field equation for the displacements:

$$\bar{E}\left[\frac{1-\nu}{2}u_{\alpha,\beta\beta} + \frac{1+\nu}{2}u_{\beta,\beta\alpha}\right] = \frac{\mu}{hH}u_\alpha. \tag{12}$$

An inspection of this equation suggests a length scale:

$$l = \sqrt{hH\bar{E}/\mu}. \tag{13}$$

Its significance is described as follows.

Consider a crack, much longer than l, running on the x_1-axis. In the crack wake, the displacement field is one-dimensional: $u_1 = 0$ and $u_2 = u_2(x_2)$, reducing Eq. (12)

to an ordinary differential equation, $\mathrm{d}^2u_2/\mathrm{d}x_2^2 = u_2/l^2$, and the traction-free boundary condition to $\sigma + \bar{E}\,\mathrm{d}u_2/\mathrm{d}x_2 = 0$ at $x_2 = 0$. In the region $x_2 > 0$, we find that $u_2(x_2) = (l\sigma/\bar{E})\exp(-x_2/l)$, $\sigma_{22}(x_2) = \sigma[1-\exp(-x_2/l)]$, and $\tau_2(x_2) = \sigma\sqrt{(\mu h)/(\bar{E}H)}\exp(-x_2/l)$. The fields vary exponentially, with l being the characteristic length.

The wake of the long crack opens by $2u_2(0^+) = 2l\sigma/\bar{E}$. When the crack extends by a unit length, the reduction in the elastic energy equals the difference between the elastic energy in a unit slice of the structure far ahead the crack tip and that far behind: $h\sigma u_2(0^+) = h\sigma^2 l/\bar{E}$. By definition, the energy release rate of the crack, G, is the elastic energy reduction associated with the crack advancing a unit area, so that $G = \sigma^2 l/\bar{E}$. Under the plane stress conditions, the stress intensity factor relates to the energy release rate as $G = K^2/E$ (Irwin, 1957). Consequently, the stress intensity factor for a long crack is (Xia and Hutchinson, 2000)

$$K = \sigma[(1-\nu^2)l]^{1/2}. \tag{14}$$

This stress intensity factor scales with the shear modulus of the underlayer as $K \propto \mu^{-1/4}$. The underlayer constrains the crack: the stiffer the underlayer, the shorter the length l, the smaller the crack wake opening, and the smaller the stress intensity factor.

For a finite crack, length $2a$, the stress intensity factor depends on the ratio $\alpha = a/l$, taking the form

$$K = \sigma[(1-\nu^2)l]^{1/2}k(a/l). \tag{15}$$

The function k also depends on Poisson's ratio. When $a/l \to \infty$, the crack is long and $k(\infty) = 1$. When $a/l \to 0$, the underlayer has a negligible stiffness, so that the film is effectively free-standing, $K = \sigma\sqrt{\pi a}$, and $k(\alpha) \to \sqrt{\pi\alpha/(1-\nu^2)}$ as $\alpha \to 0$. The function

$$k(\alpha) = \frac{1-\exp\left[-b_1\sqrt{\pi\alpha/(1-\nu^2)}\right]}{1+(b_1-1)\exp\left[-b_2\sqrt{\pi\alpha/(1-\nu^2)}\right]} \tag{16}$$

approaches both asymptotic limits, where b_1 and b_2 are fitting parameters. Fig. 2 compares this function ($b_1 = 5.8, b_2 = 3.3$) to the numerical solution of Xia and Hutchinson (2000) for Poisson's ratio $\nu = 0.3$. The crack is effectively semi-infinite when $a > l$.

3.2. Viscoelastic underlayer

For a viscoelastic underlayer, at time $t = 0^+$, the glassy elastic state prevails, with modulus μ_0, and the stress intensity factor is

$$K_0 = \sigma[(1-\nu^2)l_0]^{1/2}k(a/l_0), \quad \text{with } l_0 = \sqrt{hH\bar{E}/\mu_0}. \tag{17}$$

At time $t = \infty$, the rubbery elastic state prevails, with modulus μ_∞, and the stress intensity factor is

$$K_\infty = \sigma[(1-\nu^2)l_\infty]^{1/2}k(a/l_\infty), \quad \text{with } l_\infty = \sqrt{hH\bar{E}/\mu_\infty}. \tag{18}$$

A typical cross-linked polymer varies its modulus by four orders of magnitude: $\mu_0 \sim 10^9$ N/m^2 and $\mu_\infty \sim 10^5$ N/m^2. Consequently, $l_\infty/l_0 = (\mu_0/\mu_\infty)^{1/2} \sim 10^2$. For a short

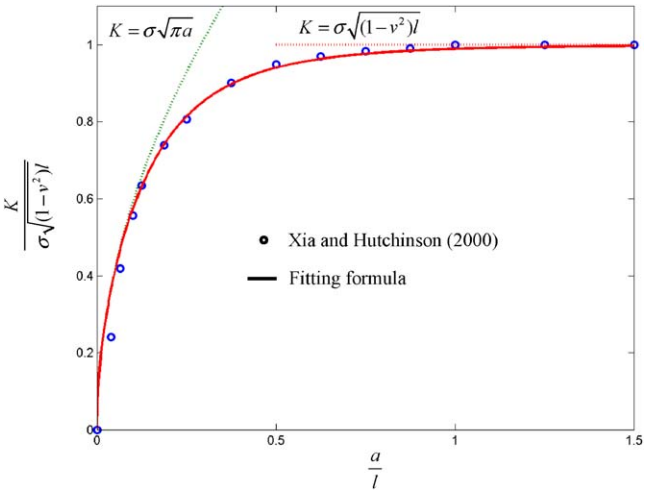

Fig. 2. The stress intensity factor for a crack, length $2a$, in a brittle film on an elastic underlayer. The dashed curve and line are the asymptotes. The solid curve is a fit to the numerical results of Xia and Hutchinson (2000).

crack, $a \ll l_0$, the underlayer is so compliant that the film is effectively free-standing, and the stress intensity factor is time-independent, $K = \sigma\sqrt{\pi a}$. For a long crack, $a \gg l_\infty$, as the underlayer creeps, the stress intensity factor increases from $K_0 = \sigma[(1-\nu^2)l_0]^{1/2}$ to $K_\infty = \sigma[(1-\nu^2)l_\infty]^{1/2}$, so that $K_\infty/K_0 = (\mu_0/\mu_\infty)^{1/4} \sim 10$.

We now classify crack initiation behaviors. Let the initial crack length be $2a_I$. At time $t = 0^+$, the stress intensity factor is $K_0(a_I)$, Eq. (17). If $K_0(a_I) > K_{th}$, the crack initiates its growth instantaneously. Otherwise, if $K_0(a_I) < K_{th}$, the crack will not initiate instantaneously. As time goes on, the underlayer creeps, and the stress intensity factor increases, approaching $K_\infty(a_I)$, Eq. (18). If $K_\infty(a_I) < K_{th}$, the crack remains stationary forever. If $K_0(a_I) < K_{th} < K_\infty(a_I)$, however, the crack initiates its growth after a delay. Fig. 3 maps the three behaviors on the plane spanned by dimensionless parameters a_I/l_0 and $K_{th}/\sigma\sqrt{(1-\nu^2)l_0}$. The two parameters measure the initial crack length and the film stress, everything else being fixed for a given tri-layer structure.

Fig. 4 maps three crack growth behaviors on the plane spanned by the same two dimensionless parameters. As before, the crack will never grow if $K_\infty(a_I) < K_{th}$. Below the curve, the crack will grow. Once initiated in an infinite film, the crack will never slow down. Reinterpreting Eq. (14), we note that $\sigma\sqrt{(1-\nu^2)l_0}$ is the stress intensity factor for a long crack running at a high velocity, so that the underlayer has no time to creep. Within our model, when $\sigma\sqrt{(1-\nu^2)l_0} > K_c$, the crack will accelerate to infinite velocity. When $\sigma\sqrt{(1-\nu^2)l_0} < K_c$, the crack will attain a steady state, in which the crack velocity and the stress intensity factor remain constant. Both the steady stress intensity factor and the steady crack velocity depend on the viscoelastic relaxation function, as well as on the subcritical crack growth law.

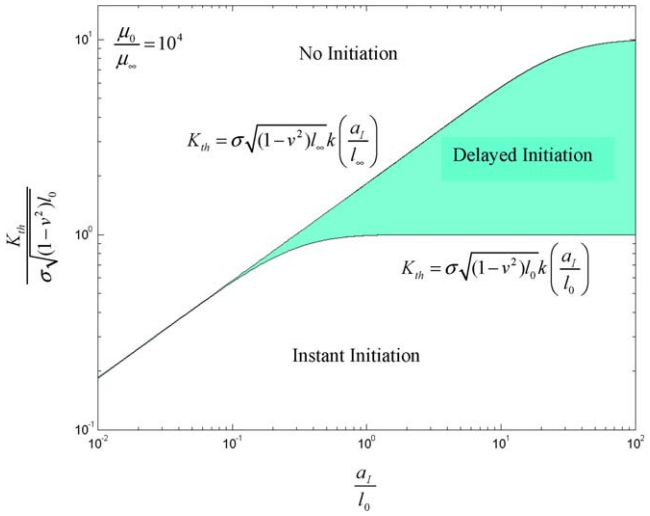

Fig. 3. The map of crack initiation behaviors, on the coordinate plane of the normalized initial crack length and the normalized threshold stress intensity factor. Set $\mu_0/\mu_\infty = 10^4$.

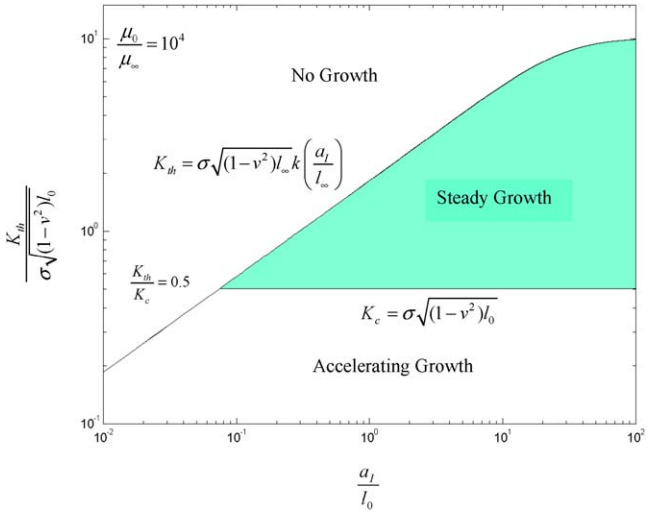

Fig. 4. The map of crack growth behaviors. Set $\mu_0/\mu_\infty = 10^4$ and $K_{\mathrm{th}}/K_{\mathrm{c}} = 0.5$.

4. Delayed crack initiation

When the crack tip is stationary, as the underlayer creeps, the stress intensity factor is a function of time, $K(t)$. The crack initiates after a delay time t_{I}, which is reached when $K(t_{\mathrm{I}}) = K_{\mathrm{th}}$.

By definition, the Laplace transform of the time-dependent function $\mu(t)$ is

$$\hat{\mu}(s) = \int_0^\infty \mu(t)\exp(-st)\,\mathrm{d}t. \tag{19}$$

Denote the Laplace transform of the displacement field by $\hat{u}_\alpha(x_1, x_2, s)$. Following the convolution theorem (Christensen, 1982), we transform Eq. (6) to

$$\bar{E}\left(\frac{1-\nu}{2}\hat{u}_{\alpha,\beta\beta} + \frac{1+\nu}{2}\hat{u}_{\beta,\beta\alpha}\right) = \frac{s\hat{\mu}}{hH}\hat{u}_\alpha. \tag{20}$$

The traction-free boundary condition, Eq. (7), is transformed to

$$\sigma n_\alpha + s\bar{E}\left[\frac{(1-\nu)}{2}(\hat{u}_{\alpha,\beta} + \hat{u}_{\beta,\alpha}) + \nu\hat{u}_{\gamma,\gamma}\delta_{\alpha\beta}\right] n_\beta = 0. \tag{21}$$

Comparing Eq. (20) with (12), and (21) with (7), we note that the boundary value problem with the transformed viscoelastic underlayer is identical to that with an elastic underlayer, using the substitutions $u \to s\hat{u}$, $\mu \to s\hat{\mu}(s)$, $K \to s\hat{K}(s)$, etc.

Rewriting Eqs. (15) and (13), we obtain the transformed stress intensity factor:

$$\hat{K}(s) = \frac{\sigma}{s}[(1-\nu^2)l(s)]^{1/2}k\left(\frac{a}{l(s)}\right), \quad \text{with } l(s) = \sqrt{hH\bar{E}/(s\hat{\mu}(s))}. \tag{22}$$

Once the relaxation function $\mu(t)$ is prescribed, one can calculate its Laplace transform $\hat{\mu}(s)$. An inverse Laplace transform of (22) gives the stress intensity factor as function of time, $K(t)$. Lehner et al. (1981) obtained an analytical expression similar to Eq. (22) for a simplified model. The use of the Laplace transform in solving viscoelastic boundary value problems is well known. Less appreciated is its use for structures that integrate elastic, viscous, and viscoelastic materials.

Experimentally measured relaxation function $\mu(t)$ can be interpreted in terms of a spring-dashpot array (Fig. 5). To ensure a rubbery elastic limit, one parallel component must be a spring of modulus μ_∞, without dashpot. Each of the other parallel components, comprising a spring of modulus μ_m and a dashpot of viscosity η_m, models a mode of molecular response with the relaxation parameter $p_m = \mu_m/\eta_m$. In the glassy limit, when the time is so short that all the dashpots have no displacements, $\mu_0 = \mu_\infty + \mu_1 + \mu_2 + \cdots$. The spring-dashpot array leads to the relaxation function (Christensen, 1982):

$$\mu(t) = \mu_\infty + \mu_1\exp(-p_1 t) + \mu_2\exp(-p_2 t) + \cdots. \tag{23}$$

The array is a general representation of viscoelastic deformation in that it can generate any relaxation function $\mu(t)$, provided the array has a sufficient number of components. The Laplace transform of the relaxation function is

$$\hat{\mu}(s) = \frac{\mu_\infty}{s} + \frac{\mu_1}{s+p_1} + \frac{\mu_2}{s+p_2} + \cdots. \tag{24}$$

4.1. Semi-infinite crack, viscous underlayer

Huang et al. (2002a) have studied cracks in a brittle film on a viscous underlayer using a finite element method. We now solve the problem using the Laplace transform.

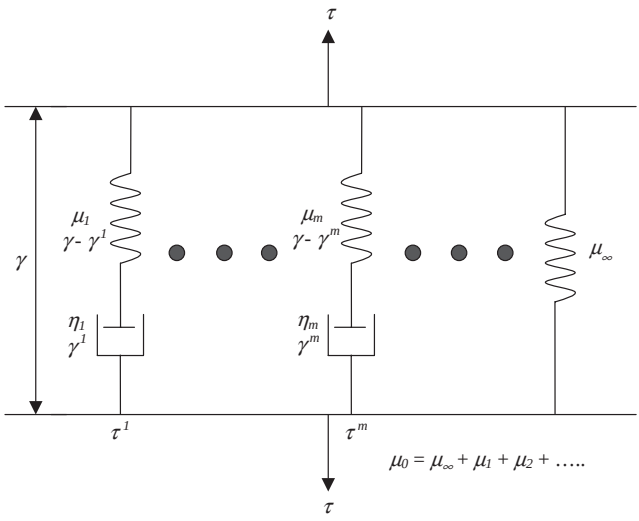

Fig. 5. A spring-dashpot array represents underlayer viscoelastic deformation.

The Laplace transform of the relaxation function is $\hat{\mu}(s)=\eta$. For a semi-infinite crack, $k=1$ in Eq. (22), and the inverse Laplace transform is obtained analytically, giving

$$K(t)=1.103\sigma\sqrt{1-\nu^2}(hH\bar{E}t/\eta)^{1/4}. \tag{25}$$

The numerical factor is an approximate value of the gamma function $\Gamma(5/4)$. Comparing to this analytical result, the finite element results in Huang et al. (2002a) are accurate to a few percent.

When the underlayer is viscous, the stress intensity factor for the semi-infinite crack vanishes at $t=0$, and is unbounded as $t\to\infty$. Consequently, the crack will initiate its growth after a delay, when the stress intensity factor rises to the threshold value, $K=K_{\mathrm{th}}$. Eq. (25) shows that the delay time scales with the stress as $t_1\sim\sigma^{-4}$. In the wake of the long crack, the displacement field is one-dimensional, governed by the diffusion-like equation: $\mathrm{d}u_2/\mathrm{d}t=(HhE/\eta)\,\mathrm{d}^2u_2/\mathrm{d}x_2^2$, with the effective diffusivity $D=HhE/\eta$. The length, $\sqrt{tD}=\sqrt{HhEt/\eta}$, scales the crack wake region in which the stress is relaxed. The same length enters Eq. (25).

4.2. Finite crack, viscous underlayer

In this and the following cases, we will use a numerical method to compute the inverse Laplace transform (Knight and Raiche, 1982). For a finite crack in the brittle film on the viscous layer, Fig. 6 plots the stress intensity factor. The problem now has two length scales: the crack length $2a$, and the diffusion length $(t\bar{E}hH/\eta)^{1/2}$. Indicated in Fig. 6 are two asymptotes. When $(hH\bar{E}t/\eta)^{1/2}/a\ll 1$, the film relaxes in the small zone near the crack, and the crack is effectively infinitely long, so that Eq. (25) applies. When $(hH\bar{E}t/\eta)^{1/2}/a\gg 1$, the film relaxes in a large region, and the crack is similar

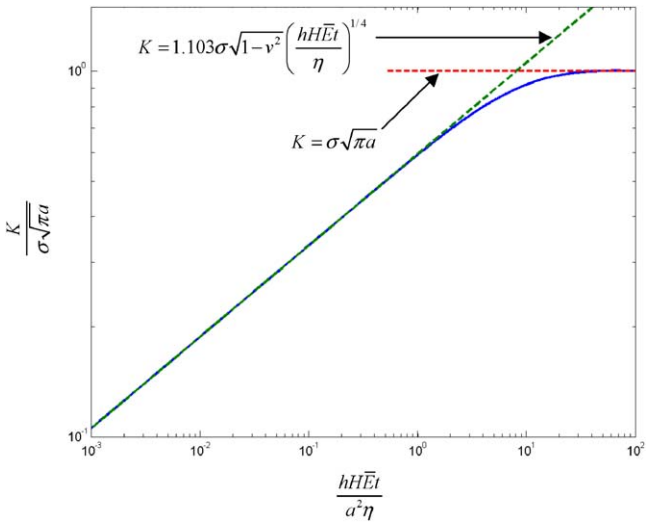

Fig. 6. The stress intensity factor of a crack, length $2a$, in an elastic film on a viscous underlayer. The dashed lines are the asymptotes. The solid curve is obtained by the inverse Laplace transform.

to the one in a free-standing sheet, $K = \sigma\sqrt{\pi a}$. If $K_{\text{th}} > \sigma\sqrt{\pi a}$, the crack will remain stationary forever. If $K_{\text{th}} < \sigma\sqrt{\pi a}$, the crack will initiate its growth after a delay.

4.3. Semi-infinite crack, viscoelastic underlayer

In all numerical calculation involving a viscoelastic underlayer, we will only use first two terms in Eq. (23), corresponding to the spring μ_∞, the spring μ_1, and the dashpot η_1 in Fig. 5. The glassy modulus is $\mu_0 = \mu_\infty + \mu_1$, and the relaxation parameter is $p_1 = \mu_1/\eta_1 = (\mu_0 - \mu_\infty)/\eta_1$.

A crack is effectively semi-infinite if $a > l_\infty$, and $\hat{K}(s)$ is given by (22), with $k = 1$. Fig. 7 plots $K(t)$ for $\mu_0/\mu_\infty = 2^4, 5^4, 10^4$. As time increases, the stress intensity factor increases from the glassy limit, $\sigma\sqrt{(1-\nu^2)l_0}$, to the rubbery limit, $\sigma\sqrt{(1-\nu^2)l_\infty}$. The characteristic time for the $K(t)$ function, say the time to reach the average of the two limits, $t_{0.5}$, increases with μ_0/μ_∞. When the two elastic limits are far apart, $\mu_0/\mu_\infty \gg 1$, the stress intensity factor rises according to the power law derived for the viscous underlayer, $K \sim t^{1/4}$.

4.4. Finite crack, viscoelastic underlayer

For a finite crack, the glassy limit is given by Eq. (17), and the rubbery limit by Eq. (18). Fig. 8 plots $K(t)$ for several crack sizes, with the modulus ratio fixed at $\mu_0/\mu_\infty = 10^4$. When the crack is long, $a/l_0 \gg 1$, the stress intensity factor rises according to the power law derived for the viscous underlayer, $K \sim t^{1/4}$.

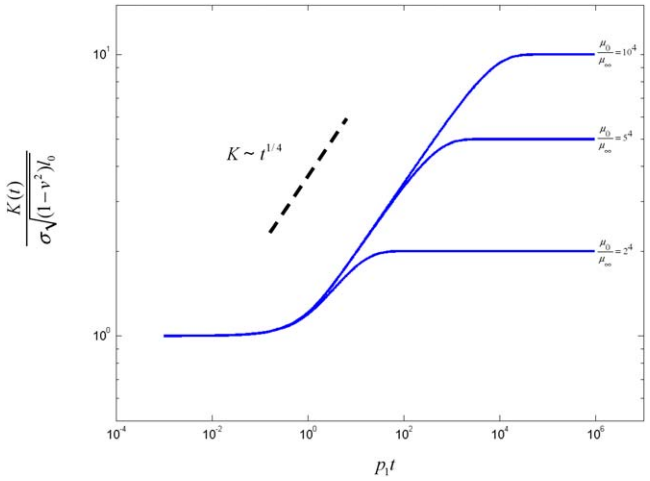

Fig. 7. The stress intensity factor of a semi-infinite crack in a brittle film on a viscoelastic underlayer.

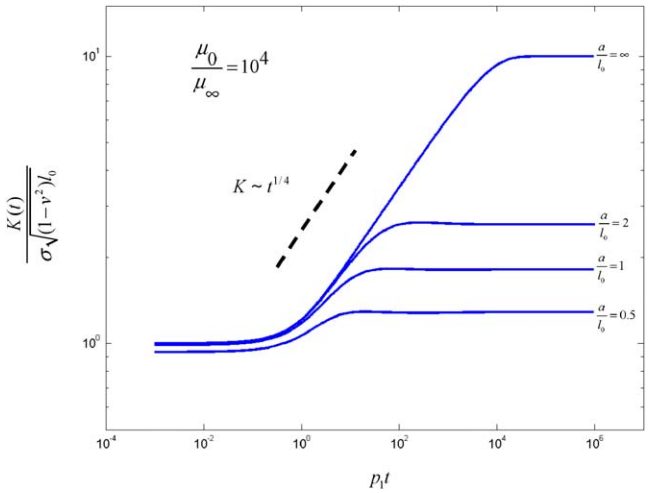

Fig. 8. The stress intensity factor of a crack, length $2a$, in a brittle film on a viscoelastic underlayer ($\mu_0/\mu_\infty = 10^4$).

5. Steady crack growth

5.1. Elastic underlayer

First assume that the underlayer is elastic, with shear modulus μ and the length scale $l = \sqrt{\bar{E}hH/\mu}$. A crack, initial length $2a_I$, remains stationary forever if $\sigma[(1-\nu^2)l]^{1/2}k(a_I/l) < K_{th}$, and grows instantaneously otherwise. In the latter case, when

the crack length becomes $2a$, the stress intensity factor is $K = \sigma[(1-\nu^2)l]^{1/2}k(a/l)$, setting the crack velocity according to the subcritical crack growth law $V(K)$. When the crack is long compared to l, the stress intensity factor approaches an asymptotic value $\sigma\sqrt{(1-\nu^2)l}$. If $\sigma\sqrt{(1-\nu^2)l} < K_c$, the crack will attain a steady state, with the stress intensity factor $K_{ss} = \sigma\sqrt{(1-\nu^2)l}$ and the crack velocity $V_{ss} = V(K_{ss})$. If $\sigma\sqrt{(1-\nu^2)l} > K_c$, however, the crack velocity is not limited by the subcritical growth law, but by factors outside the present model, such as inertia.

5.2. Viscous underlayer

Next consider a viscous underlayer with viscosity η. At time $t=0$, the underlayer allows no crack opening, so that the stress intensity factor is zero and the crack is stationary. After some time, the crack will grow if $K_{th} < \sigma\sqrt{\pi a_1}$; otherwise the crack will remain stationary forever. When the crack tip moves slowly, the crack wake has a long time to relax, and the stress intensity around the crack tip increases. When the crack tip moves rapidly, the crack wake has a short time to relax, and the stress intensity around the crack tip decreases. Consequently, the crack can attain a steady velocity. By dimensional analysis, Liang et al. (2003b) showed that the steady-state velocity scales as

$$V_{ss} = \chi \frac{Hh\bar{E}\sigma^2}{\eta K_{ss}^2}, \tag{26}$$

where χ is a dimensionless number depending on Poisson's ratio. An numerical analysis gave $\chi \approx 0.5$ for $\nu = 0.3$. As expected, the larger the crack velocity, the smaller the stress intensity factor, $V_{ss} \sim K_{ss}^{-2}$. The intersection of the two curves, Eq. (26) and the subcritical crack growth law $V(K)$, determines the steady state values V_{ss} and K_{ss}. When the underlayer is viscous, the crack, once initiated to grow, will always reach a steady state. The numerical analysis of Liang et al. (2003b) showed that the steady state is reached when the crack grows by a length on the order $(K_{ss}/\sigma)^2$.

5.3. Viscoelastic underlayer

When the crack tip moves, the Laplace transform method described in Section 4 is inapplicable. Lehner et al. (1981) obtained the steady crack velocity for a simplified model using an analytical method. In this paper, we evolve the underlayer viscoelastic deformation and the subcritical crack using a finite element method outlined in the appendix. The method also allows us to study transient cracks, and patterns of multiple cracks.

If the dimensionless parameters fall into the shaded region in Fig. 4, the crack will attain a steady state velocity, V_{ss}, and the stress intensity factor will attain a steady state value, K_{ss}. Dimensional considerations dictate that the steady crack velocity relate to the steady stress intensity factor as

$$\frac{V_{ss}}{p_1 l_0} = f\left(\frac{\mu_0}{\mu_\infty}, \frac{K_{ss}}{\sigma\sqrt{(1-\nu^2)l_0}}\right). \tag{27}$$

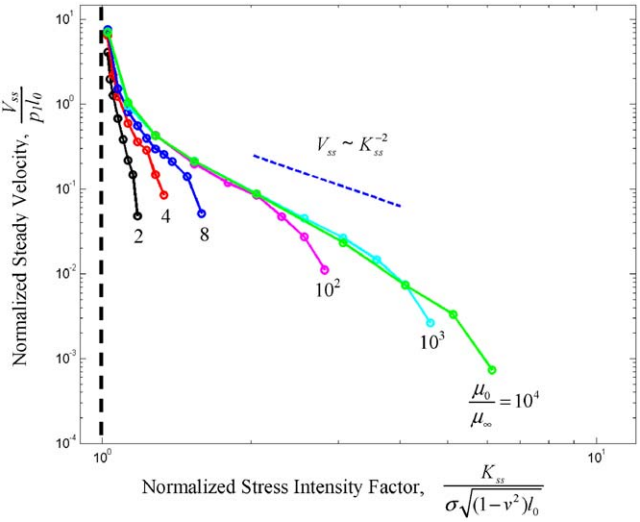

Fig. 9. Steady crack velocity versus steady stress intensity factor.

The subcritical crack growth law does not enter Eq. (27). Fig. 9 plots the $V_{ss}-K_{ss}$ curve for several values of μ_0/μ_∞, calculated using the finite element method. When $V_{ss} \to 0$, the underlayer has a long time to creep, and $K_{ss} = \sigma\sqrt{(1-\nu^2)l_\infty}$. When $V_{ss} \to \infty$, the underlayer has no time to creep, and $K_{ss} = \sigma\sqrt{(1-\nu^2)l_0}$. For $\mu_0/\mu_\infty = 1$, the $V_{ss} - K_{ss}$ curve recovers the elastic limit and becomes vertical. For larger μ_0/μ_∞, the $V_{ss} - K_{ss}$ curve approaches the viscous limit $V_{ss} \sim K_{ss}^{-2}$. In each case, the steady state exists if the $V_{ss} - K_{ss}$ curve intersects with the subcritical crack growth law $V(K)$.

6. Transient crack growth

In all the above calculations, we need not explicitly specify the subcritical crack growth law. In this section, to simulate the transient crack growth, we assume that

$$\frac{da}{dt} = \begin{cases} 0, & K < K_{th} \\ V_0(K/K_c)^n, & K_{th} < K < K_c \\ \infty, & K > K_c \end{cases} \tag{28}$$

with the numerical values $n = 10, K_{th}/K_c = 0.1$, and $V_0/(p_1 l_0) = 1$. The underlayer has one relaxation mode, with $\mu_0/\mu_\infty = 10^2$. The finite element method is used to evolve the crack and deformation simultaneously.

Fig. 10 plots the crack velocity as a function of time for two cases. In both cases, the initial crack size is $a_1/l_0 = 0.2$, and the crack initiates its growth instantaneously. For case A, $K_c/\left(\sigma\sqrt{(1-\nu^2)l_0}\right) = 1.5$, and the approaches a steady state. For Case B, $K_c/\left(\sigma\sqrt{(1-\nu^2)l_0}\right) = 0.8$, and the crack accelerates without bound.

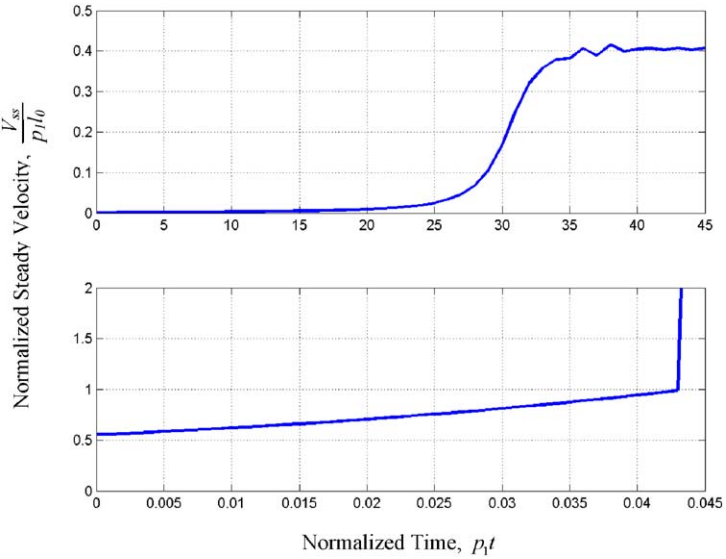

Fig. 10. The transient crack velocity as a function of time.

We finally consider a case of multiple cracks. Fig. 11a shows the initial crack configuration, with the coordinates given in units of l_0. The underlayer deforms with the glassy modulus. Contours of the stress component σ_{22}/σ display the field in the film. Figs. 11b and c plot the contours at two later times. Only the two outer cracks grow. The three inner cracks are shielded and remain stationary.

7. Concluding remarks

In an integrated structure, creep in one material affects fracture in another material. This paper analyzes a tri-layer structure, invoking two rate processes: subcritical crack growth in the thin film, and viscoelastic deformation in the underlayer. We map crack behaviors using a small set of parameters. When the crack tip is stationary, as the underlayer creeps, the stress intensity factor increases. We calculate the stress intensity factor as a function of time using a Laplace transform. The result gives the time for delayed crack initiation. When the crack tip moves, the crack length and the displacement field co-evolve. Within our model, the crack either attains a steady state or accelerates unbounded. An extended finite element method is formulated to evolve patterns of multiple cracks with a relative course mesh, and without remeshing. It is hoped that these results will help in planning experiments for time-dependent fracture and deformation in integrated structures, and in interpreting accelerated reliability tests of organic-containing devices.

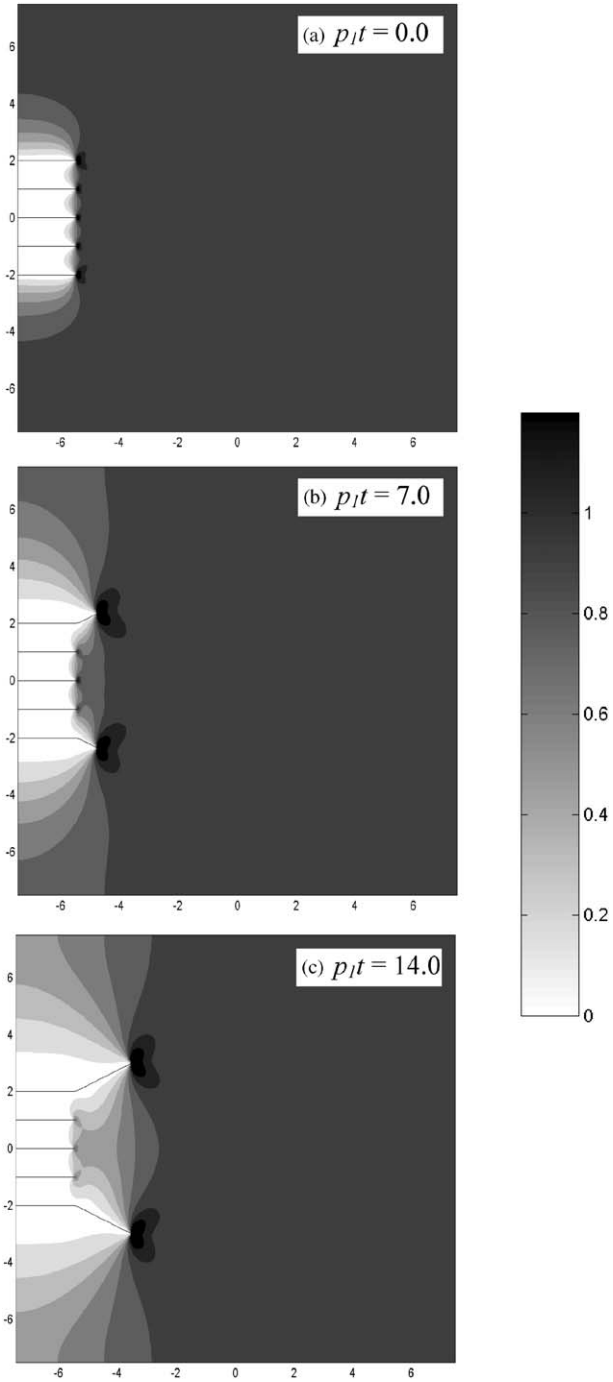

Fig. 11. Several cracks pre-exist in the film. The contour plots of the stress component σ_{22} display the evolution. Only the two outer cracks grow.

Acknowledgements

This paper is prepared for a symposium held at Caltech, 16–18 January 2003, organized by A.J. Rosakis, G. Ravichandran, and S. Suresh, to celebrate the 60th birthday of Professor L.B. Freund. Discussions with Rui Huang, of the University of Texas at Austin, and Jun He, of Intel Corporation, are helpful. Our work in this area is supported partly by the National Science Foundation through grants CMS-9820713 and CMS-9988788 with Drs. K. Chong and J. Larsen-Basse as Program Directors, and partly by the New Jersey Commission for Science and Technology.

Appendix A. Nonequilibrium thermodynamic model of co-evolution

The physics of the model is better conveyed in the language of nonequilibrium thermodynamics. The results lead naturally to a finite element method. Represent the viscoelastic underlayer by the spring-dashpot array in Fig. 5, and denote the strain due to dashpot m by γ_α^m. The structure in Fig. 1 is a nonequilibrium thermodynamic system. Specify its configuration by a set of *kinematic variables*: the in-plane displacements u_α, the dashpot strains γ_α^m, and the crack length a. The in-plane strains in the film are $\varepsilon_{\alpha\beta} = (u_{\alpha,\beta} + u_{\beta,\alpha})/2$, and the shear strains in the underlayer, $\gamma_\alpha = u_\alpha/H$. The object is to evolve the kinematic variables.

We next specify *energetics*. The elastic energy per unit volume of the film is

$$w = \sigma\varepsilon_{\alpha\alpha} + \frac{1}{2}\bar{E}[(1-v)\varepsilon_{\alpha\beta}\varepsilon_{\alpha\beta} + v(\varepsilon_{\gamma\gamma})^2], \tag{A.1}$$

In the spring-dashpot array (Fig. 5), the total strain is γ_α, the strain of dashpot m is γ_α^m, and the strain of spring m is $\gamma_\alpha - \gamma_\alpha^m$. The elastic energy per unit volume of the underlayer is the sum of the contributions from all the springs:

$$W = \frac{1}{2}\mu_\infty\gamma_\alpha\gamma_\alpha + \frac{1}{2}\mu_1(\gamma_\alpha - \gamma_\alpha^1)(\gamma_\alpha - \gamma_\alpha^1) + \frac{1}{2}\mu_2(\gamma_\alpha - \gamma_\alpha^2)(\gamma_\alpha - \gamma_\alpha^2) + \cdots. \tag{A.2}$$

The total energy of the system is the integral over the entire film area:

$$U = \int (hw + HW)\,\mathrm{d}A. \tag{A.3}$$

The system evolves to reduce the total energy.

We finally specify *kinetics*. When the kinematic variables vary by δu_α, $\delta\gamma_\alpha^m$ and δa, the energy varies by

$$\delta U = \int (h\sigma_{\alpha\beta}\delta u_{\alpha,\beta} + \tau_\alpha\delta u_\alpha)\,\mathrm{d}A - \int H(\tau_\alpha^1\delta\gamma_\alpha^1 + \tau_\alpha^2\delta\gamma_\alpha^2 + \cdots)\,\mathrm{d}A - hG\delta a. \tag{A.4}$$

This equation places all the kinematic variables on the equal footing. The differential coefficients are the driving forces associated with the kinematic variables. Their physical significance is described as follows, term by term.

The first integral in Eq. (A.4) is the energy variation associated with the in-plane displacements δu_α. The in-plane stresses $\sigma_{\alpha\beta}$ are given by

$$\sigma_{\alpha\beta} = \sigma\delta_{\alpha\beta} + \bar{E}\left[\frac{1-\nu}{2}(u_{\alpha,\beta} + u_{\beta,\alpha}) + \nu u_{\gamma,\gamma}\delta_{\alpha\beta}\right]. \tag{A.5}$$

The shear stresses in the underlayer are given by

$$\tau_\alpha = \mu_0\frac{u_\alpha}{H} - \mu_1\gamma_\alpha^1 - \mu_2\gamma_\alpha^2 + \cdots. \tag{A.6}$$

The system is in force balance, so that the energy variation with the in-plane displacements vanishes:

$$\int (h\sigma_{\alpha\beta}\delta u_{\alpha,\beta} + \tau_\alpha\delta u_\alpha)\,\mathrm{d}A = 0. \tag{A.7}$$

This variational statement is the basis for the finite element method. The statement also reproduces the force balance equation (1), as well as the traction-free boundary condition (7).

The second integral in Eq. (A.4) is the energy variation with the dashpot strains $\delta\gamma_\alpha^m$. The associated driving force is the stress acting on component m in the spring-dashpot array, τ_α^m, which relates to the kinematic variables as

$$\tau_\alpha^m = \mu^m\left(\frac{u_\alpha}{H} - \gamma_\alpha^m\right). \tag{A.8}$$

Creep is a nonequilibrium process. Assume that the dashpot strain-rate is linear in the shear stress: $\partial\gamma_\alpha^m/\partial t = \tau_\alpha^m/\eta_m$. So long as the viscosity is positive, creep dissipates energy, as confirmed by Eq. (A.4). Combining with Eq. (A.8), this kinetic law leads to a set of ordinary differential equations to evolve the dashpot strains:

$$\frac{\partial\gamma_\alpha^m}{\partial t} = p_m\left(\frac{u_\alpha}{H} - \gamma_\alpha^m\right). \tag{A.9}$$

Generalization to nonlinear creep is straightforward within this framework.

The last term in Eq. (A.4) is the energy variation with the crack length δa. The energy release rate is

$$G = \int (wn_1 - \sigma_{\alpha\beta}n_\beta u_{\alpha,1})\,\mathrm{d}S + \int (\tau_\alpha/h)u_{\alpha,1}\,\mathrm{d}A. \tag{A.10}$$

In Eq. (A.10), the first integral is carried over a curve that starts on one crack face, and ends on another crack face; this integral is the J-integral (Rice, 1968). The second integral extends over the area enclosed by the curve. The term $-\tau_\alpha/h$ acts like a body force in the plane of the film, so that Eq. (A.10) is the path-independent integral that includes the body force (Kishmoto et al., 1980). Once the energy release is calculated from Eq. (A.10), the stress intensity factor is given by the Irwin relation, $G = K^2/E$, and the crack length a evolves according to the subcritical crack growth law, $\mathrm{d}a/\mathrm{d}t = V(K)$. The crack extension also dissipates energy, as evident in Eq. (A.4).

We evolve the structure according to the following algorithm. At a given time t_n, know the values of all the kinematic variables: the in-plane displacements, the dashpot strains, and the crack length. In the interval $\Delta t = t_{n+1} - t_n$, assume that the in-plane

displacements increase with time linearly, and integrate Eq. (A.9) analytically, giving

$$\gamma_\alpha^m(t_{n+1}) = \mathrm{e}^{-p_m\Delta t}\gamma_\alpha^m(t_n) + \left(\frac{1-\mathrm{e}^{-p_m\Delta t}}{p_m\Delta t} - \mathrm{e}^{-p_m\Delta t}\right)\frac{u_\alpha(t_n)}{H} + \left(1 - \frac{1-\mathrm{e}^{-p_m\Delta t}}{p_m\Delta t}\right)\frac{u_\alpha(t_{n+1})}{H}. \tag{A.11}$$

Update the shear stresses according to Eq. (A.6), and the crack length according to the subcritical crack growth law. Solve the plane stress problem at t_{n+1} according to the variational statement (A.7) to determine the displacements $u_\alpha(t_{n+1})$. Repeat the procedure for many time increments to evolve the structure over a long time. Following Moës et al. (1999), we implement an extended finite element method (XFEM) in a general-purpose finite element package DYNAFLOW (Prévost, 1981). Additional details can be found in Liang et al. (2003a, b), where we have treated elastic and viscous underlayer separately.

References

Ambrico, J.M., Jones, E.E., Begley, M.R., 2002. Cracking in thin multi-layers with finite-width and periodic architectures. Int. J. Solids Struct. 39, 1443–1462.

Arzt, E., 1998. Size effects in materials due to microstructural and dimensional constraints: a comparative review. Acta Mater. 46, 5611–5626.

Beuth, J.L., 1992. Cracking of thin bonded films in residual tension. Int. J. Solids Struct. 29, 1657–1675.

Beuth, J.L., Klingbeil, N.W., 1996. Cracking of thin films bonded to elastic-plastic substrates. J. Mech. Phys. Solids 44, 1411–1428.

Cairns, D.R., Witte, R.P., Sparacin, D.K., Sachsman, S.M., Paine, D.C., Crawford, G.P., 2000. Strain-dependent electrical resistance of tin-doped indium oxide on polymer substrates. Appl. Phys. Lett. 76, 1425–1427.

Christensen, R.M., 1982. Theory of Viscoelasticity: An Introduction. Academic Press, New York.

Cook, R.F., Liniger, E.G., 1999. Stress-corrosion cracking of low-dielectric-constant spin-on-glass thin films. J. Electochem. Soc. 146, 4439–4448.

Dauskardt, R.H., Lane, M., Ma, Q., Krishna, N., 1998. Adhesion and debonding of multi-layer thin film structures. Eng. Fract. Mech. 61, 141–162.

Elsasser, W.M., 1969. Convection and stress propagation in the upper mantle. In: Runcorn, W.K. (Ed.), The Application of Modern Physics to Earth and Planetary Interiors. Wiley, New York, pp. 223–246.

Evans, A.G., Hutchinson, J.W., 1995. The thermomechanical integrity of thin films and multilayers. Acta Metall. Mater. 43, 2507–2530.

Forrest, S.R., 1997. Ultrathin organic films grown by organic molecular beam deposition and related techniques. Chem. Rev. 97, 1793–1896.

Freund, L.B., 1990. Dynamic Fracture Mechanics. Cambridge University Press, Cambridge, UK.

Freund, L.B., 1994. The mechanics of dislocations in strained-layer semiconductor materials. Adv. Appl. Mech. 30, 1–66.

Freund, L.B., 2000. The mechanics of electronic materials. Int. J. Solids Struct. 37, 185–196.

Freund, L.B., Nix, W.D. Unpublished research.

Freund, L.B., Suresh, S., 2003. Thin Films and Layered Materials: Stress, Deformation and Fracture. Cambridge University Press, Cambridge, UK, to be published.

Gao, H., Nix, W.D., 1999. Surface roughening of heteroepitaxial thin films. Annual Rev. Mater. Sci. 29, 173–209.

Gleskova, H., Wagner, S., Suo, Z., 1999. Stability of amorphous silicon transistors under extreme in-plane strain. Appl. Phys. Lett. 75, 3011–3013.

He, J., 2002. Unpublished research.
He, J., Morris, W.L., Shaw, M.C., Mather, J.C., Sridhar, N., 1998. Reliability in large area solder joint assemblies and effects of thermal expansion mismatch and die size. Int. Microelectron. Packag. Soc. 21, 297–305.
Hsu, P.I., Bhattacharya, R., Gleskova, H., Huang, M., Xi, Z., Suo, Z., Wagner, S., Sturm, J.C., 2002. Thin-film transistor circuits on large-area spherical surface. Appl. Phys. Lett. 81, 1723–1725.
Hu, M.S., Evans, A.G., 1989. The cracking and decohesion of thin films on ductile substrates. Acta Metall. 37, 917–925.
Huang, R., Yin, H., Liang, J., Hobart, K.D., Sturm, J.C., Suo, Z., 2001. Relaxation of a strained elastic film on a viscous layer. Mater. Res. Soc. Symp. Proc. 695, 115–120.
Huang, R., Prévost, J.H., Suo, Z., 2002a. Loss of constraint on fracture in thin film structures due to creep. Acta Mater. 50, 4137–4148.
Huang, M., Suo, Z., Ma, Q., 2002b. Ratcheting induced cracks in thin film structures. J. Mech. Phys. Solids 50, 1079–1098.
Hutchinson, J.W., Evans, A.G., 2000. Mechanics of materials: top-down approaches to fracture. Acta Mater. 48, 125–135.
Hutchinson, J.W., Suo, Z., 1991. Mixed-mode cracking in layered materials. Adv. Appl. Mech. 29, 63–191.
Irwin, G.R., 1957. Analysis of stresses and strains near the end of a crack traversing a plate. J. Appl. Mech. 24, 361–364.
Kishmoto, K., Aoki, S., Sakata, M., 1980. On the path independent integral $\hat{J}$. Eng. Fract. Mech. 13, 841–850.
Knauss, W., 1970. Delayed failure—the Griffith problem for linearly viscoelastic materials. Int. J. Fract. Mech. 6, 7–20.
Knight, J.H., Raiche, A.P., 1982. Transient electromagnetic calculations using the Gaver-Stehfest inverse Laplace transform method. Geophysics 47, 47–50.
Lawn, B., 1993. Fracture of Brittle Solids, Second Edition. Cambridge University Press, Cambridge.
Lehner, F.K., Li, V.C., Rice, J.R., 1981. Stress diffusion along rupture plate boundaries. J. Geophys. Res. 86, 6155–6169.
Liang, J., Huang, R., Prévost, J.H., Suo, Z., 2003a. Evolving crack patterns in thin films with the extended finite element method. Int. J. Solids Structures, in press. (Preprint available online at http://www.princeton.edu/∼suo, Publication 137)
Liang, J., Huang, R., Prévost, J.H., Suo, Z., 2003b. Thin film cracking modulated by underlayer creep. Exp. Mech., in press. (Preprint available online at http://www.princeton.edu/∼suo, Publication 132)
Ma, Q., Xie, J., Chao, S., El-Mansy, S., McFadden, R., Fujimoto, H., 1998. Channel cracking technique for toughness measurement of brittle dielectric thin films on silicon substrates. Mater. Res. Soc. Symp. Proc. 516, 331–336.
Martin, S.J., Godschalx, J.P., Mills, M.E., Shaffer II, E.O., Townsend, P.H., 2000. Development of a low-dielectric-constant polymer for the fabrication of integrated circuit interconnect. Adv. Mater. 12, 1769–1778.
McElhaney, K.W., Ma, Q., 2003. Investigation of moisture-assisted SiO_2 films using a channel cracking technique. Manuscript in preparation.
Moës, N., Dolbow, J., Belytschko, T., 1999. A finite element method for crack growth without remeshing. Int. J. Numer. Methods Eng. 46, 131–150.
Moran, P.D., Kuech, T.F., 2001. Kinetics of strain relaxation in semiconductor films grown on borosilicate glass-bonded substrates. J. Electron. Mater. 30, 802–806.
Nix, W.D., 1989. Mechanical-properties of thin-films. Metall. Trans. 20A, 2217–2245.
Prévost, J.H., 1981. DYNAFLOW: A Nonlinear Transient Finite Element Analysis Program. Princeton University, last updated in 2003.
Rice, J.R., 1968. Mathematical analysis in the mechanics of fracture. In: H. Liebowitz (Ed.), Fracture—An Advanced Treatise, Vol. II. Academic Press, New York, pp. 191–308.
Rice, J.R., 1980. The mechanics of earthquake rupture. In: Dziewonski, A.M., Boschi, E. (Eds.), Physics of the Earth's Interior. Italian Physical Society/North-Holland, Amsterdam, pp. 555–649.
Sridhar, N., Srolovitz, D.J., Cox, B.N., 2002. Buckling and post-buckling kinetics of compressed thin films on viscous substrates. Acta Mater. 50, 2547–2557.

Suo, Z., 1997. Motions of microscopic surfaces in materials. Adv. Appl. Mech. 33, 193–294.

Suo, Z., 2003. Reliability of interconnect structures. In: Gerberich, W., Yang, W. (Eds.), A Manuscript prepared as a chapter in Volume 8: Interfacial and Nanoscale Failure. In: Milne, I., Ritchie, R.O., Karihaloo, B. (Editors-in-Chief). Comprehensive Structural Integrity. Due for publication early 2003. (Preprint available online at http://www.princeton.edu/∼suo, Publication 139)

Volinsky, A.A., Moody, N.R., Gerberich, W.W., 2002. Interfacial toughness measurements for thin films on substrates. Acta Mater. 50, 441–466.

Xia, Z.C., Hutchinson, J.W., 2000. Crack patterns in thin films. J. Mech. Phys. Solids 48, 1107–1131.